Mouse monoclonal antibodies against SRC-1 were purified from hybridoma culture supernatants using a mAb TRAP GII column (Pharmacia). Analysis of various GST–SRC fusion proteins by western blotting with purified SRC-1 mAb 677-F11 indicates that the antibody epitope maps to the region encompassing residues 840 to 947 but not to GST. Western blots were visualized using goat anti-mouse secondary antibodies conjugated to alkaline phosphatase followed by chemoluminescence detection with an ECL kit (Amersham Life Science).

IP-HAT assays. Immunoprecipitation (IP)-HAT assays were done as described[7]. The HAT assay was incubated at 30 °C for 30–45 min. Histone acetylation was measured using a P-81 filter-binding assay as described[9].

Protein expression and purification. cDNAs corresponding to portions of SRC-1 or CBP were excised from human SRC-1 and mouse CBP using restriction endonucleases and subcloned into either the *E. coli* expression plasmid pRSET-GST (InVitrogen), yeast expression plasmid pCBUBGST[24] or baculovirus expression plasmid pVLGST (InVitrogen). Portions of SRC-1 were expressed as GST fusion proteins in *E. coli* (amino acids (aa) 383–568, 383–841, 782–1,139, 1,027–1,139, 1,139–1,250, 1,027–1,250, 1,107–1,441), yeast (aa 1–399, 1,216–1,441) or insect cells (aa 383–841, 1,107–1,441). The PCAF interaction region of CBP (aa 1,775–2,008) was expressed as a GST fusion protein in *E. coli*. Recombinant GST–SRC and GST–CBP fusion proteins were affinity-purified from these whole-cell extracts with gluthathione–Sepharose 4B beads (Pharmacia). Protein concentration was determined using the Bradford protein assay (BioRad), and the purity of the full-length protein was assessed by Coomassie blue staining of 12% SDS–PAGE minigels.

Liquid HAT assays. Liquid assays for HAT activity were done essentially as described. Chicken mononucleosomes stripped of H1 and H5 were prepared as described previously[9]. Histone amino-terminal peptides with a C-terminal cysteine and histone amino-terminal MAP peptides[25] were obtained from the protein core facility at Baylor College of Medicine. Synthetic histone amino-terminal peptides were acetylated as described[9], with 300 ng peptide per reaction and an incubation time of 20 min.

***In vitro* interaction assay.** For *in vitro* transcription and translation, Flag PCAF[6] was subcloned in pCR 3.1 (InVitrogen). About 50 pmol of purified GST–SRC fusion proteins was incubated with 20 μl glutathione–Sepharose beads (Pharmacia) in suspension for 2 h at 4 °C. Resins were then washed twice with $NETN_{1000}$ (20 mM Tris-HCl, pH 7.5, 1 mM EDTA, 0.5% NP-40, 100 mM NaCl). Subsequently, beads were mixed with 5 μl of *in vitro* transcribed and translated [^{35}S]methionine-labelled Flag–PCAF crude lysate (Promega), and reacted for 1 hour. Beads were then washed six times with $NETN_{100}$. Bound radiolabelled protein was separated on 10% SDS–PAGE gels and detected by fluorography.

Mammalian two-hybrid assay. Flag-PCAF[6] was subcloned into the pAB-GalDBD vector[5] to express the Gal4 DNA-binding domain (residues 1 to 147) fused to full-length PCAF. Portions of SRC-1 were subcloned in-frame into the pABVP16 vector which expresses the VP16 activation domain. HeLa cells were transfected with Gal-PCAF, VP16-SRC, and $(UAS)_4$TATA-luciferase[19] reporter plasmids as described[17]. Cell extracts were assayed for luciferase activity and values were corrected for protein concentration. Data are represented as fold induction (±s.d.) of triplicate values obtained from a representative experiment which was independently repeated at least three times.

Received 25 June; accepted 29 July 1997.

1. Klein-Hitpass, L. *et al.* The progesterone receptor stimulates cell-free transcription by enhancing the formation of a stable preinitiation complex. *Cell* **60,** 247–257 (1990).
2. Brownell, J. E. & Allis, C. D. Special HATs for special occasions: linking histone acetylation to chromatin assembly and gene activation. *Curr. Opin. Genet. Dev.* **6,** 176–184 (1996).
3. Wolffe, A. P. & Pruss, D. Targeting chromatin disruption: transcription regulators that acetylate histones. *Cell* **86,** 817–819 (1996).
4. Wade, P. A. & Wolffe, A. P. Histone acetyltransferases in control. *Curr. Biol.* **7,** R82–R84 (1997).
5. Onate, S. A., Tsai, S. Y., Tsai, M.-J. & O'Malley, B. W. Sequence and characterization of a coactivator for the steroid hormone receptor superfamily. *Science* **270,** 1354–1357 (1995).
6. Yang, X.-J. *et al.* A p300/CBP-associated factor that competes with the adenoviral oncoprotein E1A. *Nature* **382,** 319–324 (1996).
7. Bannister, A. J. & Kouzarides, T. The CBP co-activator is a histone acetyltransferase. *Nature* **384,** 641–643 (1996).
8. Ogryzko, V. V. *et al.* The transcriptional coactivators p300 and CBP are histone acetyltransferases. *Cell* **87,** 953–959 (1996).
9. Mizzen, C. A. *et al.* The $TAF_{II}250$ subunit of TFIID has histone acetyltransferase activity. *Cell* **87,** 1261–1270 (1996).
10. Brownell, J. E. *et al. Tetrahymena* histone acetyltransferase A: a homolog to yeast Gcn5p linking histone acetylation to gene activation. *Cell* **84,** 843–852 (1996).
11. Candau, R., Zhou, J. X., Allis, C. D. & Berger, S. L. Histone accetyltransferase activity and interaction with ADA2 are critical for GCN5 function *in vivo*. *EMBO J.* **16,** 555–565 (1997).
12. Archer, T. K., Lefebvre, P., Wolford, R. D. & Hager, G. L. Transcription factor loading on the MMTV promoter: a bimodal mechanism for promoter activation. *Science* **255,** 1573–1576 (1992).
13. Truss, M. *et al.* Hormone induces binding of receptors and transcription factors to a rearranged nucleosome on the MMTV promoter *in vivo*. *EMBO J.* **14,** 1737–1751 (1995).
14. Felsenfeld, G. *et al.* Chromatin structure and gene expression. *Proc. Natl Acad. Sci. USA* **93,** 9384–9388 (1996).
15. Wong, J., Shi, Y-B. & Wolffe, A. P. A role for nucleosome assembly in both silencing and activation of the *Xenopus* TRβA gene by the thyroid hormone receptor. *Genes Dev.* **9,** 2696–2711 (1995).
16. Wolffe, A. P. Nucleosome positioning and modification: chromatin structures that potentiate transcription. *Trends Biochem. Sci.* **9,** 240–244 (1994).
17. Jenster, G. *et al.* Steroid receptor induction of gene transcription: a two-step model. *Proc. Natl Acad. Sci. USA* **94,** 7879–7884 (1997).
18. Kamei, Y. *et al.* A CBP integrator complex mediates transcriptional activation and AP-1 inhibition by nuclear receptors. *Cell* **85,** 403–414 (1996).
19. Smith, C. S., Onate, S. A., Tsai, M.-J. & O'Malley, B. W. CREB binding protein acts synergistically with steroid receptor coactivator-1 to enhance steroid receptor-dependent transcription. *Proc. Natl Acad. Sci. USA* **93,** 8884–8888 (1996).
20. Wong, J., Shi, Y-B. & Wolffe, A. P. Determinants of chromatin disruption and transcriptional regulation instigated by the thyroid hormone receptor: hormone regulated chromatin disruption is not sufficient for transcriptional activation. *EMBO J.* **11,** 3158–3171 (1997).
21. Wolffe, A. P. Histone deacetylase: a regulator of transcription. *Science* **272,** 371–372 (1996).
22. Taunton, J., Hassig, C. A. & Schreiber, S. L. A mammalian histone deacetylase related to a yeast transcriptional regulator Rpd3. *Science* **272,** 408–411 (1996).
23. Kingston, R. E., Bunker, C. A. & Imbalzano, A. M. Repression and activation by multiprotein complexes that alter chromatin structure. *Genes Dev.* **10,** 950–920 (1996).
24. Baniahmad, A. *et al.* Interaction of human thyroid hormone receptor beta with transcription factor TFIIB may mediate target gene derepression and activation by thyroid hormone. *Proc. Natl Acad. Sci. USA* **90,** 8832–8836 (1993).
25. Tam, J. P. Synthetic peptide vaccine design: synthesis and properties of a high-density multiple antigenic peptide system. *Proc. Natl Acad. Sci. USA* **85,** 5409–5413 (1988).
26. Brownell, J. E. & Allis, C. D. An activity gel assay detects a single, catalytically active histone acetyltransferase subunit in *Tetrahymena* macronuclei. *Proc. Natl Acad. Sci. USA* **92,** 6364–6368 (1995).

Acknowledgements. We thank P. Samora and L. Gong for technical support of the experiments; D. P. Edwards for assistance with monoclonal antibody production; Y. Nakatani for the human Flag-PCAF plasmid; and A. Wolffe and J. Wong for discussion. This work was supported by an NIH NRSA postdoctoral fellowship (T.E.S.), a TALENT stipend from the Netherlands Organization for Scientific Research (G.J.) and an NIH grant (B.W.O.).

Correspondence and requests for materials should be addressed to B.W.O. (e-mail: berto@bcm.tmc.edu).

Molecular mechanics of calcium–myristoyl switches

James B. Ames*, Rieko Ishima†, Toshiyuki Tanaka‡, Jeffrey I. Gordon§, Lubert Stryer* & Mitsuhiko Ikura†‡

** Department of Neurobiology, Stanford University School of Medicine, Stanford, California 94305, USA*
† Division of Molecular and Structural Biology, Ontario Cancer Institute and Department of Medical Biophysics, University of Toronto, 610 University Avenue, Toronto, Ontario, M5G 2M9, Canada
‡ Center for Tsukuba Advanced Research Alliance and Institute of Applied Biochemistry, University of Tsukuba, Tsukuba 305, Japan
§ Department of Molecular Biology and Pharmacology, Washington University School of Medicine, St Louis, Missouri 63110, USA

Many eukaryotic cellular and viral proteins have a covalently attached myristoyl group at the amino terminus. One such protein is recoverin, a calcium sensor in retinal rod cells, which controls the lifetime of photoexcited rhodopsin by inhibiting rhodopsin kinase[1–6]. Recoverin has a relative molecular mass of 23,000 (M_r 23K), and contains an amino-terminal myristoyl group (or related acyl group) and four EF hands[7]. The binding of two Ca^{2+} ions to recoverin leads to its translocation from the cytosol to the disc membrane[8,9]. In the Ca^{2+}-free state, the myristoyl group is sequestered in a deep hydrophobic box, where it is clamped by multiple residues contributed by three of the EF hands[10]. We have used nuclear magnetic resonance to show that Ca^{2+} induces the unclamping and extrusion of the myristoyl group, enabling it to interact with a lipid bilayer membrane. The transition is also accompanied by a 45-degree rotation of the amino-terminal domain relative to the carboxy-terminal domain, and many hydrophobic residues are exposed. The conservation of the myr-

istoyl binding site and two swivels in recoverin homologues from yeast to humans indicates that calcium–myristoyl switches are ancient devices for controlling calcium-sensitive processes.

The observation that viral Src protein is oncogenic only when myristoylated demonstrates the biological importance of this hydrophobic modification[11]. More recently, it was found that calcium induces the binding of myristoylated, but not unmyristoylated, recoverin to membranes, suggesting that recoverin possesses a calcium–myristoyl switch[8,9]. It was proposed that the myristoyl group is sequestered in the calcium-free form of the protein and becomes exposed in the calcium-bound form, enabling it to insert into a membrane or a hydrophobic site of a target protein. These experiments suggested that myristoyl groups are not simply hydrophobic anchors, but can serve as dynamic partners in signalling.

X-ray crystallographic studies of recombinant unmyristoylated recoverin showed it to contain a compact array of four EF hands, which contrasts with the dumb-bell shape of calmodulin and troponin C[12]. In crystal form, Ca^{2+} was bound to EF-3, the high-affinity site, but not to EF-2, the low-affinity site. The other two EF hands cannot bind Ca^{2+}: EF-1 is disabled by a Cys-Pro sequence at a critical loop position, and EF-4 is disabled by an internal Lys-Glu salt bridge. Myristoylated recoverin, the physiologically active form, has thus far have eluded crystallization. We therefore turned to nuclear magnetic resonance (NMR) spectroscopy to solve the structure of both its calcium-free and calcium-bound state. In the calcium-free state, the myristoyl group is sequestered in a deep hydrophobic cavity in the N-terminal domain[10]. The cavity is formed by aromatic and other non-polar residues contributed by five flanking helices. The tight hairpin turn between the N-terminal helix and the sequestered myristoyl group gave the impression of a cocked trigger. NMR studies of the environment of the myristoyl group then demonstrated that Ca^{2+} induces the extrusion of the myristoyl group[13,14].

The next step in unravelling the mechanism of the calcium switch was to obtain a structure of the entire protein in the Ca^{2+}-bound state. Determining the complete structure proved to be problematic because the Ca^{2+}-bound form is considerably less soluble than the Ca^{2+}-free form. This difficulty was circumvented by making an analogue of myristoylated recoverin with oxygen in place of carbon at position 13 of the fatty-acyl chain. Recoverin bearing this myristoyl analogue has a functional calcium–myristoyl switch and is sufficiently soluble to allow its structure to be fully determined by NMR spectroscopy. The relationship of the structure of this 13-oxa analogue to myristoylated recoverin was ascertained by obtaining heteronuclear single quantum coherence spectra of both proteins, which serve as fingerprints of the conformation of their

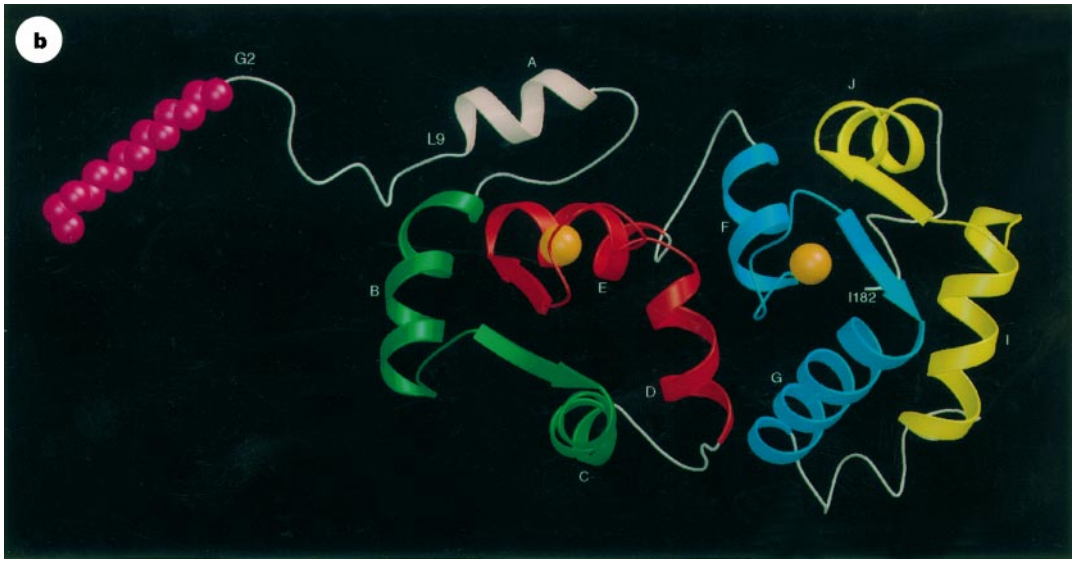

Figure 1 a, Superposition of the main-chain atoms of the 24 NMR-derived structures of myristoylated recoverin with two Ca^{2+} bound. The 13-oxa myristoyl group (magenta), bound Ca^{2+} (orange), and the four EF-hands (green, red, cyan and yellow) are indicated. The r.m.s. deviation of the NMR-derived structures relative to the mean structure is 0.8 ± 0.1 Å for main-chain atoms and 1.35 ± 0.1 Å for all non-hydrogen atoms in the helical regions. This figure was generated using Midas[27]. **b**, Schematic ribbon representation of the energy-minimized average structure of Ca^{2+}-bound myristoylated recoverin. The average position of the myristoyl group is shown as a space-filling model. Helices (A, residues 9–18; B, 27–38; C, 46–56; D, 64–73; E, 83–93; F, 102–109; G, 119–132; H, 135–140; I, 148–160; J, 169–178; K, 181–187) are labelled and the colour scheme is as **a**. The figure was generated using Molscript[28] and Raster3d[29].

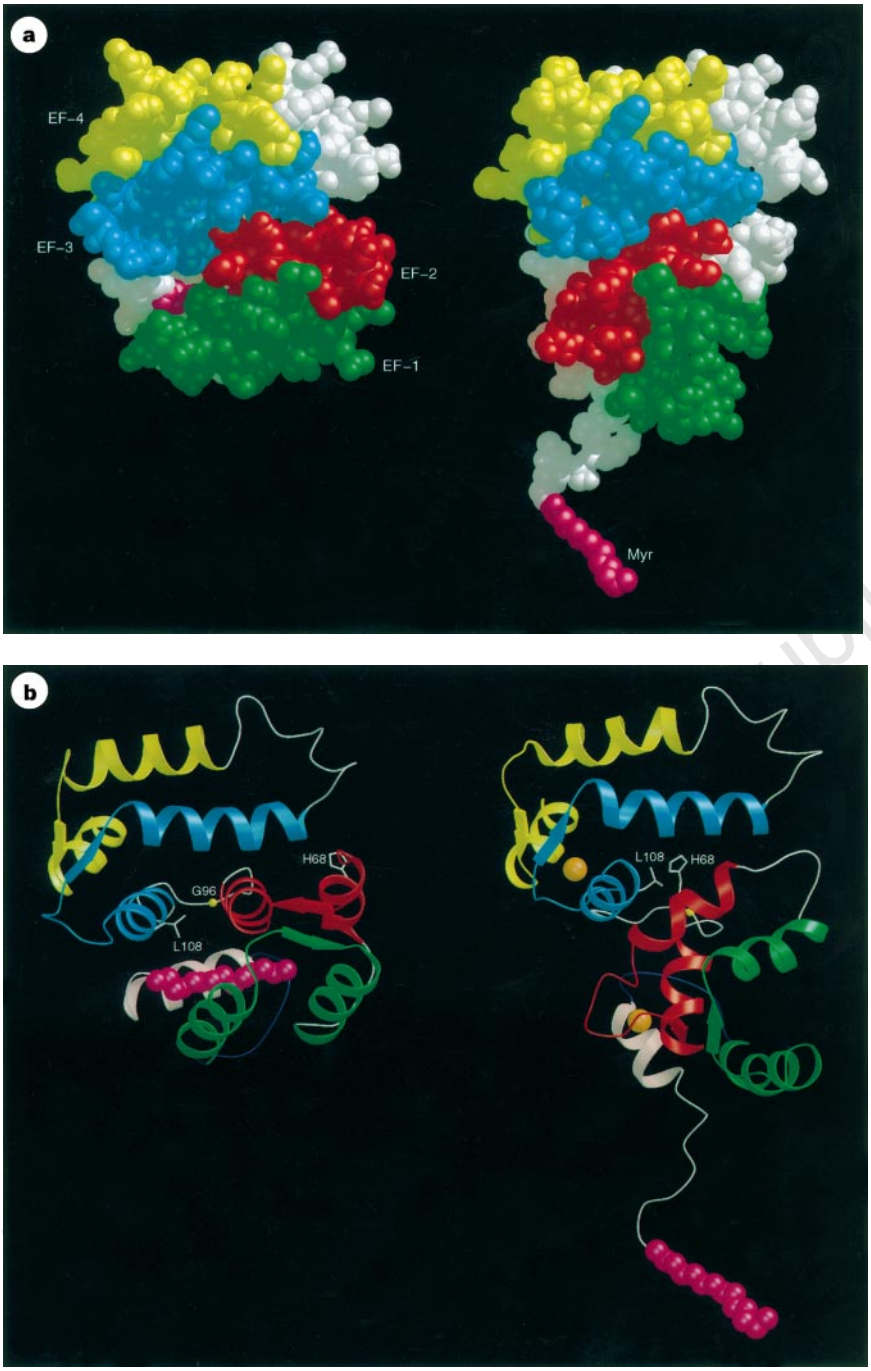

Figure 2 Space-filling model (**a**) and ribbon diagram (**b**) of Ca^{2+}-free[10] (left, liku.pdb) and Ca^{2+}-bound (right) myristoylated recoverin. The C-terminal domains of the two forms are aligned to show the Ca^{2+}-induced 45-deg rotation of the N-terminal domain.

main-chain and side-chain amide groups. The near identity of these spectra indicates that the structure of the 13-oxa analogue is almost the same as that of myristoylated recoverin.

A superposition of 24 NMR-derived structures of Ca^{2+}-bound myristoylated recoverin is shown in Fig. 1a, and their average is depicted as a ribbon diagram in Fig. 1b. The myristoyl group is clearly extruded in aqueous solution, where it occupies many different positions. The N-terminal eight residues of the Ca^{2+}-bound form are also disordered and exposed to the solvent. Thus the N-terminal region serves as a mobile arm to position the myristoyl group outside the protein when Ca^{2+} is bound. This flexible arm is followed by a short α-helix that precedes the four EF-hand motifs, which are arranged in a linear array. EF-1 and EF-2 interact intimately to form the N-terminal domain, and EF-3 and EF-4 interact to form the C-terminal domain. The last 13 residues are disordered. Ca^{2+} is bound to EF-2 and EF3. EF-3 has the conformation of a classic EF hand, but EF-2 is rather different. The root-mean-squared (r.m.s.) deviations of the main-chain atoms of these EF hands and those of Ca^{2+}-bound calmodulin are <1.2 and 3.7 Å, respectively. The overall topology of Ca^{2+}-bound myristoylated recoverin is similar to that of unmyristoylated recoverin containing one bound Ca^{2+}.

The structures of the Ca^{2+}-free[10] and Ca^{2+}-bound forms of myristoylated recoverin are compared in Fig. 2. The C-terminal domains of the two forms are quite similar, apart from changes in the Ca^{2+}-binding loop and the entering helix of EF-3. The N-terminal domain, by contrast, undergoes a striking rearrangement caused by rotation of the backbone at Gly 42, which is located in the loop between the helices of EF-1. Rotation about this swivel markedly changes the interhelical angle of EF-1. In the Ca^{2+}-bound

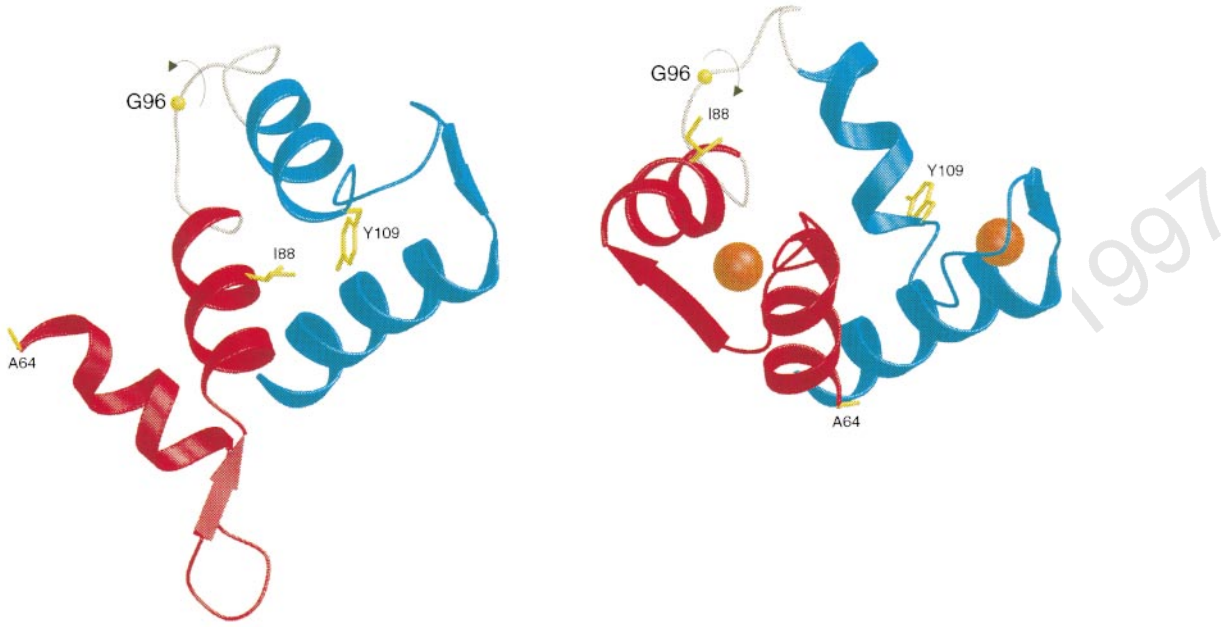

Figure 3 Schematic ribbon representation of the structure of EF-2 and EF-3 of Ca^{2+}-free (left) and Ca^{2+}-bound (right) myristoylated recoverin. Rotation about Gly 96 dramatically alters the interaction between EF-2 and EF-3, as highlighted by the displacement of Ile 88 and Tyr 109. The ϕ and ψ angles of Gly 96 are 135° and –161° (Ca^{2+}-free), and 73° and –178° (Ca^{2+}-bound), respectively.

state, EF-1, like EF-3, adopts an open conformation akin to that of the Ca^{2+}-occupied EF hands in calmodulin and troponin C[15,16]. The transition to the open conformation exposes hydrophobic residues, enabling them to interact with a target. Another important consequence of this rotation is the unclamping of the myristoyl group. Ejection of the myristoyl group is further promoted by the Ca^{2+}-induced melting of the N-terminal helix to provide a flexible arm. Extrusion of the myristoyl group requires the binding of Ca^{2+} to EF-2 and EF-3 (refs 8, 17). But how is the occupancy of EF-3 in the C-terminal domain communicated to the myristoyl group in the N-terminal domain? The binding of Ca^{2+} to EF-2 and EF-3 induces structural changes in these EF hands, rather like those seen in calmodulin and troponin C[16,18]. The weakened interaction of these EF hands at the domain interface promotes a conformational change near Gly 96 in the U-shaped interdomain linker. The interface between the two domains is rearranged completely by rotation at Gly 96, which serves as a second swivel. Ca^{2+} binding leads to a rotation of 45 deg of one domain with respect to the other (Fig. 2).

The structural consequences of Ca^{2+}-induced rotation at Gly 96 between domains are highlighted in Fig. 3. In the Ca^{2+}-free state, the exiting helix of EF-2 contains a series of hydrophobic residues (Ile 88, Ala 89, His 91 and Met 92) that interact with hydrophobic residues in both the entering and exiting helices of EF-3 (Leu 108, Tyr 109, Ile 125 and Ala 128). The entering helix of EF-2 is exposed to solvent in the Ca^{2+}-free protein, and does not interact with EF-3. Conversely, in the Ca^{2+}-bound protein, the entering helix of EF-2 (marked by Ala 64 in Fig. 3) interacts intimately with EF-3, whereas the exiting helix of EF-2 (marked by Ile 88 in Fig. 3) does not. In particular, Ala 64, Tyr 65 and His 68 of the EF-2 entering helix interact with the hydrophobic residues Leu 108, Ile 125, Ala 128 and Met 132 of EF-3. Furthermore, the loops of EF-2 and EF-3 are 20 Å closer when Ca^{2+} is bound. The switching of helices accompanying the domain rotation accounts for the cooperativity of Ca^{2+} binding to EF-2 and EF-3.

The second important swivel is at Gly 42 in the loop between the helices of EF-1 (Fig. 4). Rotation here moves the entering helix of EF-1 outwards causing it to pull on residues Gly 2 to Glu 26 on the N-terminal side of the helix. This displacement allows the myristoyl

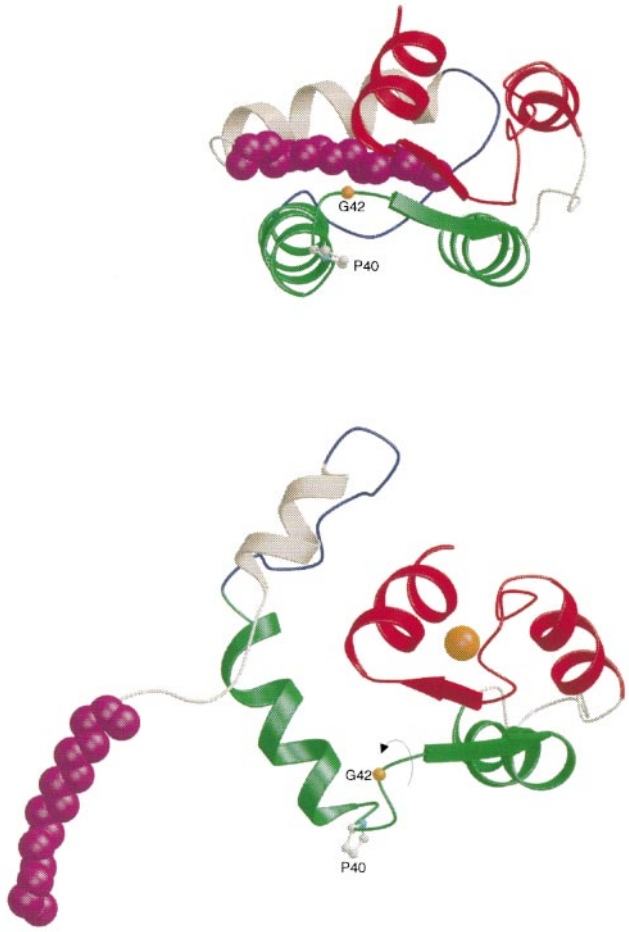

Figure 4 Schematic ribbon representation of the structure of the N-terminal domain of Ca^{2+}-free (top) and Ca^{2+}-bound (bottom) recoverin. Rotation about Gly 42 enables the extrusion of the myristoyl group.

group to swing out of its binding pocket. The unclamping of the myristoyl group is also essential for its extrusion. Many aromatic and other hydrophobic residues (notably Leu 28, Trp 31, Tyr 32, Ile 52, Phe 49, Tyr 53, Phe 56, Tyr 86, Leu 90, Trp 104 and Leu 108) fit snugly around the myristoyl group in the Ca^{2+}-free state. The binding of Ca^{2+} causes several clamping residues (Leu 14, Leu 28, Tyr 32, Trp 104 and Leu 108) to move apart. Ejection of the myristoyl group is also made possible by the melting of part of the N-terminal helix. In the Ca^{2+}-free form, the long amphipathic N-terminal helix (Lys 5 to Glu 16) fits tightly against and is stabilized by the sequestered myristoyl group. In the Ca^{2+}-bound state, residues Gly 2 to Ala 8 have become part of the flexible arm that places the myristoyl group outside and gives it freedom to insert into a bilayer membrane or other hydrophobic site.

More than ten homologues of recoverin have been identified in the brain. The amino-acid sequences of neurocalcins[19] and hippocalcin[20] are 55% identical to that of recoverin. These neuronal calcium sensors have been shown to possess functional calcium–myristoyl switches. The recoverin family is also present in invertebrates, as exemplified by frequenin (43% identical), which controls synaptic transmission in flies[21], and NCS (41% identical) in nematodes[22]. Indeed, yeast contains a homologue that is 45% identical to recoverin (K. Devlin, C. M. Churcher, B. G. Marrell, M. A. Rajendream and S. V. Walsh, unpublished; locus NCS1SCHPO, Swiss-Prot accession no. Q09711). Thus the recoverin family arose early in the evolution of eukaryotes. They may serve to couple calcium cascades and guanine-nucleotide-binding protein cascades. The characteristic feature of this family of calcium sensors is the presence of a myristoylation consensus sequence at the N terminus (MGXXXS), four EF-hand motifs (two or three of which bind Ca^{2+}), and CPXG (residues 39–42) in the first EF hand. Cys-Pro prevents Ca^{2+} from binding to EF-1, which instead has been recruited for a very different role, to cradle the myristoyl group and serve as part of the extrusion mechanism. The two swivels, Gly 42 in EF-1 and Gly 96 in the linker, are also conserved. Furthermore, ten residues that clamp the myristoyl group in the Ca^{2+}-free state (Trp 31, Tyr 32, Phe 49, Ile 52, Tyr 53, Phe 56 and Phe 57 in EF-1, Phe 83 and Leu 90 in EF-2, and Trp 104 in EF-3) are invariant. The high degree of conservation of residues that are important in the Ca^{2+}-induced extrusion of the myristoyl group of recoverin suggests that the calcium–myristoyl switch mechanism is almost the same in all family members, from yeast to humans. It would seem to be an ancient device for switching the location and activity of calcium sensors and modulators in signal-transduction processes. □

Methods

Sample preparation. Recombinant myristoylated recoverin with uniformly ^{15}N- and ^{13}C-labelled protein and unlabelled 13-oxa tetradecanoyl group was expressed in overproducing *Escherichia coli* strain pTrec2/pBB131/DH5α grown in M9 minimal medium and purified as described previously[8], and 13-oxa tetradecanoic acid was added (5 mg l^{-1}) 1 h before induction.

NMR spectroscopy. All NMR experiments were performed on a UNITY-plus 500 or UNITY-600 spectrometer. Sequence-specific resonance assignments were obtained for myristoylated and unmyristoylated forms of Ca^{2+}-bound recoverin[23]. Complete assignments obtained for unmyristoylated recoverin containing two bound Ca^{2+} served as a guide for assigning some resonances (about 15% of the total) of myristoylated recoverin. Structure calculations were performed using a restrained molecular dynamics stimulated annealing protocol[24] within X-PLOR[25]. A total of 2,100 inter-proton distance restraints (750 intra-residue, 470 sequential, 370 short range, and 500 long range) were obtained from nuclear Overhauser effect (NOE) spectra of myristoylated recoverin (1 mM) dissolved in 0.1 M KCl, 10 mM $CaCl_2$, 10 mM dithiothreitol, pH 7.0. In addition to the NOE-derived distance restraints, 12 distance restraints involving Ca^{2+} bound to residues in EF-2 and EF-3 (refs 12, 26), 60 distance restraints for 30 hydrogen bonds, and 266 dihedral angle restraints were included in the structure calculation. The total, experimental distance, and Lennard–Jones potential energies are 3,991, 76 and −357 kcal mol^{-1}, respectively (calculated with the use of square-well potentials for the experimental-distance empirical-energy term with a force constant of 50 kcal mol^{-1} $Å^2$). None of the distance and angle restraints were violated by more than 0.40 Å and 4.0°. The average r.m.s. deviations from an idealized geometry for bonds, angles and impropers are 0.0073 Å, 2.06° and 0.94°, respectively.

Received 24 April; accepted 10 June 1997.

1. Dizhoor, A. M. *et al.* Recoverin: a calcium sensitive activator of retinal rod guanylate cyclase. *Science* **251,** 915–918 (1991).
2. Hurley, J. B., Dizhoor, A. M., Ray, S. & Stryer, L. Recoverin's role: conclusion withdrawn. *Science* **260,** 740 (1993).
3. Gray-Keller, M. P., Polans, A. S., Palczewski, K. & Detwiler, P. B. The effect of recoverin-like calcium-binding proteins on the photoresponse of retinal rods. *Neuron* **10,** 523–531 (1993).
4. Kawamura, S., Hisatomi, O., Kayada, S., Tokunaga, F. & Kuo, C.-H. Recoverin has S-modulin activity in frog rods. *J. Biol. Chem.* **268,** 14579–14582 (1993).
5. Chen, C. K., Inglese, J., Lefkowitz, R. J. & Hurley, J. B. Ca^{2+}-dependent interaction of recoverin with rhodopsin kinase. *J. Biol. Chem.* **270,** 18060–18066 (1995).
6. Klenchin, A. K., Calvert, P. D. & Bownds, M. D. Inhibition of rhodopsin kinase by recoverin. *J. Biol. Chem.* **270,** 16147–16152 (1995).
7. Dizhoor, A. M. *et al.* The amino terminus of retinal recoverin is acylated by a small family of fatty acids. *J. Biol. Chem.* **267,** 16033–16036 (1992).
8. Zozulya, S. & Stryer, L. Calcium-myristoyl protein switch. *Proc. Natl Acad. Sci. USA* **89,** 11569–11573 (1992).
9. Dizhoor, A. M. *et al.* Role of acylated amino terminus of recoverin in Ca^{2+}-dependent membrane interaction. *Science* **259,** 829–832 (1993).
10. Tanaka, T., Ames, J. B., Harvey, T. S., Stryer, L. & Ikura, M. Sequestration of the membrane-targeting myristoyl group of recoverin in the Ca^{2+}-free state. *Nature* **376,** 444–447 (1995).
11. Kamps, M. P., Buss, J. E. & Sefton, B. M. Mutation of the amino-terminal glycine of $p60^{src}$ prevents both myristoylation and morphological transformation. *Proc. Natl Acad. Sci. USA* **82,** 4625–4628 (1985).
12. Flaherty, K. M., Zozulya, S., Stryer, L. & McKay, D. B. Three-dimensional structure of recoverin, a calcium sensor in vision. *Cell* **75,** 709–716 (1993).
13. Ames, J. B., Tanaka, T., Ikura, M. & Stryer, L. NMR evidence for Ca^{2+}-induced extrusion of the myristoyl group of recoverin. *J. Biol. Chem.* **270,** 30909–30913 (1995).
14. Hughes, R. E., Brzovic, P. S., Klevitt, R. E. & Hurley, J. B. Calcium-dependent solvation of the myristoyl group of recoverin. *Biochemistry* **34,** 11410–11416 (1995).
15. Strynadka, N. C. & James, M. N. Crystal structures of the helix-loop-helix calcium-binding proteins. *Annu. Rev. Biochem.* **58,** 951–998 (1989).
16. Ikura, M. Calcium binding and conformational response in EF-hand proteins. *Trends Biochem. Sci.* **21,** 14–17 (1996).
17. Ames, J. B., Porumb, T., Tanaka, T., Ikura, M. & Stryer, L. Amino-terminal myristoylation induces cooperative calcium binding to recoverin. *J. Biol. Chem.* **270,** 4526–4533 (1995).
18. Herzberg, O. & James, M. N. Refined crystal structure of troponin C from turkey skeletal muscle at 2.0 Å resolution. *J. Mol. Biol.* **203,** 761–779 (1988).
19. Kuno, T. *et al.* cDNA cloning of a neural visinin-like Ca^{2+}-binding protein. *Biochem. Biophys. Res. Commun.* **184,** 1219–1225 (1992).
20. Kobayashi, M., Takamatsu, K., Saitoh, S. & Noguchi, T. Molecular cloning of hippocalcin, a novel calcium-binding protein of the recoverin family. *J. Biol. Chem.* **268,** 18898–18904 (1993).
21. Pongs, O. *et al.* Frequenin: a novel calcium-binding protein that modulates synaptic efficacy in the *Drosophila* nervous system. *Neuron* **11,** 15–28 (1993).
22. De Castro, E. *et al.* Regulation of rhodopsin phosphorylation by a family of neuronal calcium sensors. *Biochem. Biophys. Res. Commun.* **216,** 133–140 (1995).
23. Ames, J. B., Tanaka, T., Stryer, L. & Ikura, M. Secondary structure of myristoylated recoverin determined by three-dimensional heteronuclear NMR: Implications for the calcium-myristoyl switch. *Biochemistry* **33,** 10743–10753 (1994).
24. Nilges, M., Gronenborn, A. M., Brunger, A. T. & Clore, G. M. Determination of three-dimensional structures of proteins by simulated annealing with interproton distance restraints. *Protein Eng.* **2,** 27–38 (1988).
25. Brunger, A. T. *X-PLOR Version 3.1: A System for X-ray Crystallography and NMR* (Yale Univ. Press, New Haven, T, 1993).
26. Babu, Y. S., Bugg, C. E. & Cook, W. J. Structure of calmodulin refined at 2.2 Å resolution. *J. Mol. Biol.* **204,** 191–199 (1988).
27. Ferrin, T., Huang, C., Jarvis, L. & Langridge, R. The MIDAS display system. *J. Mol. Graph.* **6,** 13–27 (1988).
28. Kraulis, P. J. Molscript: a program to produce both detailed and schematic plots of protein structures. *J. Appl. Crystallogr.* **24,** 946–950 (1991).
29. Bacon, D. J. & Anderson, W. F. A fast algorithm for rendering space-filling molecule pictures. *J. Mol. Graph.* **6,** 219–220 (1988).

Acknowledgements. We thank G. Gokel for help with the synthesis of 13-oxatetradecanoic acid; L. Kay for help with NMR experiments; and F. Delaglio and D. Garrett for computer software for NMR data processing and analysis. This work was supported by grants to L.S. and J.G. from the NIH, and to M.I. from the Medical Research Council of Canada. J.B.A. was supported by an NIH post-doctoral fellowship. M.I. is a Howard Hughes Medical Institute international research scholar.

Correspondence and requests for materials should be addressed to L.S. (e-mail: stryer@retina.stanford.edu) and M.I. (e-mail: mikura@oci.utoronto.ca). Coordinates have been deposited in the Brookhaven Protein Data Bank (1jsa.pdb).